Optimising Optical Performance with Ray Tracing

Bao Nguyen, Blackett Laboratory, Imperial College London.

I. Method & Testing

This paper outlines the construction of a ray tracer and its application in evaluating different optical systems. Each simulated optical system consists of a collimated input beam and a finite number of optical elements. This sub-section covers the working principles and testing of the building blocks in the simulation, which are vital in understanding the numerical investigation.

There are three implemented optical elements: spherical surface, aspheric surface and output plane. Spherical surfaces are combined to form simple lenses such as plano-convex and biconvex lenses, whilst the output plane is used to form an image at a given point. Aspheric surfaces are slightly deformed spheres used to model adaptive optics, which are discussed later. One key method of the spherical surface is the intercept, which solves (1) to determine the interception point $\vec{\mathbf{r_i}} = \vec{\mathbf{r_0}} + l\hat{\boldsymbol{k}}$, where $\vec{\mathbf{r_0}}$ is the ray's initial position. A valid intercept is the closest intercept occurring in the forward direction. When l is real, this corresponds to l_- for a convex surface and l_+ for a concave surface.

$$l_{+,-} = -\vec{\mathbf{r}} \cdot \hat{\boldsymbol{k}} \pm \sqrt{(\vec{\mathbf{r}} \cdot \hat{\boldsymbol{k}})^2 - (|\vec{r}|^2 - R^2)} \tag{1}$$

Where $\vec{\mathbf{r}}$ is the vector from the sphere's centre to the ray's initial position, $\hat{\boldsymbol{k}}$ is the normalised wave vector, and R is the radius of the sphere. Complex l indicates no intercept.

For the exception case of zero curvature (planar surface), an intercept based on (2) was used instead. If $\left|\hat{\boldsymbol{n}} \cdot \hat{\boldsymbol{k}}\right| < 10^{-6}$, the ray is essentially parallel to the plane, indicating no possible intercept. The threshold 10^{-6} is a choice that works well in the investigation but can be set lower if necessary.

$$l = \frac{|\vec{\mathbf{r_0}} - \vec{\mathbf{r_i}}|}{\left|\hat{\boldsymbol{n}} \cdot \hat{\boldsymbol{k}}\right|} \tag{2}$$

Where $\vec{\mathbf{r_0}}$ is the ray's initial position, $\vec{\mathbf{r_i}}$ is a point on the plane, and $\hat{\boldsymbol{n}}$ is the plane's normal vector.

Once the rays hit the surface, they undergo refraction modelled by Snell's law with (2), which assumes constant refractive indices in each medium. In reality, the refractive index varies as a function of wavelength due to dispersion. The refraction method terminates the ray if total internal reflection occurs. Otherwise, the ray is updated with the refracted wave vector $\hat{\boldsymbol{k_2}}$ and propagated to the surface's interception point $\vec{\mathbf{r_i}}$. Simple cases with expected output were derived to see whether the refraction method worked correctly. For instance, an incident ray from the air ($n_1 = 1$) to glass ($n_2 = 1.5$) at 45°should refract at 28°. The same incident angle from air to glass would guarantee total internal reflection, and setting $n_1 = n_2$ should ensure no refraction. The developed function successfully passed these tests, giving confidence in the physical modelling.

$$\hat{\boldsymbol{k_2}} = \frac{n_1}{n_2}[\hat{\boldsymbol{n}} \times (\hat{\boldsymbol{k_1}} \times \hat{\boldsymbol{n}})] - \hat{\boldsymbol{n}}\sqrt{1 - \left(\frac{n_1}{n_2}\right)^2 \left|\hat{\boldsymbol{n}} \times \hat{\boldsymbol{k_1}}\right|^2} \tag{3}$$

Where $\hat{\boldsymbol{k_1}}$ and $\hat{\boldsymbol{k_2}}$ are the initial and final normalised wave vector, $\hat{\boldsymbol{n}}$ is the surface's normal vector (pointing outwards) and n_1, n_2 are the refractive indices of the two mediums.

Those are the building blocks of the spherical surface class. Using this as a parent class, the aspheric surface class was created to model adaptive optics. An aspheric surface with curvature C placed at z_0 is described by (4), with the last two terms representing deviations from the spherical shape [1].

$$z(\rho) = z_0 + \frac{C\rho^2}{1 + \sqrt{1 - (C\rho)^2}} + A_4\rho^4 + A_6\rho^6 \tag{4}$$

Where $\rho = \sqrt{x^2 + y^2}$ is the radial distance from the origin, C is the surface's curvature, z_0 is the position of the surface's vertex, A_4 and A_6 are the aspheric coefficients.

The previous intercept method based on spherical geometry using (1) no longer works here. Instead, a minimisation approach was adopted, where the ray's equation is parameterised in terms of t. The algorithm searches for t_{min}, which corresponds to the minimum distance between the line and the surface. Since most adaptive optics do not deviate massively from the spherical shape [2], an initial guess t_{guess} was made based on the intercept between the ray and a spherical surface of the same curvature. The validity of this initial guess is limited to the cases with small deviations from the spherical shape (A_4, $A_6 \ll 1$) but is sufficient for the investigated physics.

For the refraction method in (3), the surface's normal vector is required, which is computed using the gradient operator. With the normal vector found, the rays are refracted and propagated to the output plane, where the RMS spot size is calculated to determine the optical performance. The RMS is calculated from polar grid sampling [3], which consists of a finite number of ray objects (N^2) confined in a cylinder of diameter D. Physically, this is a collimated beam with a diameter D, which was implemented by first generating two equally spaced arrays corresponding to the radial distance and azimuth angle. Together, these arrays form a mesh grid to generate the initial positions of rays starting at $z = 0$. From this and setting the wave vector to be (0, 0, 1), N^2 ray objects can be initialised to form a beam bundle. The validity of this method is supported by Fig 6, which shows a spot a diagram of a 5 mm collimated beam formed

by 100 rays distributed uniformly to avoid biased RMS values.

Before beginning the numerical investigation, care was taken to ensure the model functions correctly. In addition to unit tests run to test each class and function separately, the whole model was tested through simple cases with expected outputs. A negative curvature surface acts as a diverging lens, as observed in Fig 3. There should be no refraction for a surface with $n_1 = n_2$, as seen in Fig 4. Finally, a biconvex lens made up of a convex and concave surface should focus the ray to a point defined by the lens-maker equation, as found in Fig 5. This thorough testing gave confidence in the validity of the constructed ray tracer, allowing the numerical investigation to be conducted with ease.

II. Numerical Investigation

The performance of different lenses was explored using a collimated beam with $\lambda = 588$ nm. Each glass lens consists of two surfaces on the z-axis with a refractive index of 1.5168, separated by 5 mm. As seen in Fig 8 and 9, the first surface is positioned at $z = 100$ mm, while the output plane is at the paraxial focus $z \sim 198$ mm (except for one plano-convex case) to ensure a fair comparison between different lenses.

Performance of plano-convex lens

The aim here is to compare the RMS spot size associated with each orientation of the plano-convex lens for different beam diameters. A plano-convex lens consists of a curved surface and a planar surface. For the first orientation (Fig 9), the curved surface was initialised with $z_0 = 100$ mm, $C = -0.02mm^{-1}$, $n_1 = 1$, $n_2 = 1.5168$, $r_{aperture} = 50$ mm, and the planar surface was initialised with $z_0 = 105$ mm, $C = 0mm^{-1}$, $n_1 = 1.5167$, $n_2 = 1$, $r_{aperture} = 50$ mm. The second orientation (Fig 10) has similar parameters but with the surfaces swapped around. With the optical system fully set up, the beam consisting of 100 rays was initialised with a fixed diameter (1 to 10 mm with an increment of 1 mm) to determine the associated RMS spot size. A limited number of rays used for the RMS calculation led to an estimated statistical uncertainty of 10%, which is the mean difference in the RMS value when 100 and 10^6 sample rays were used. Increasing the sample size can improve the accuracy at the cost of computation time, especially for the optimisation processes later on.

The result is displayed in Fig 10, where the RMS spot size grows exponentially with the beam diameter. The orientation with the better performance is the first orientation (curved surface followed by a planar surface). The RMS spot size is in the order of 10^{-6} m, which approaches the diffraction scale of $\lambda f/D$. As the developed model only uses geometric ray optics, the subsequent investigations use a large beam diameter of 10 mm to avoid the effect of diffraction.

Optimising a biconvex lens

For a 10 mm beam, the RMS spot size of a correctly orientated plano-convex lens is 7.3 ± 0.7 μm. This was improved further with a biconvex lens consisting of a convex and concave surface. An objective function to find the associated RMS spot size was developed and minimised to find the optimal curvature combination (C_1, C_2). The searched solution was bounded to be between [0, 1/5] and [-1/5, 0] mm^{-1}, respectively, which ensures that the lens is at least 10 mm in diameter to contain the input beam. Implementing this method led to the results shown in Table I, which shows a 63% reduction in spot size.

TABLE I: Performance of optimised biconvex lens compared to plano-convex lens for a 10 mm beam.

	Plano-convex lens	Biconvex lens
C_1/mm^{-1}	0.00	1.60×10^{-2}
C_2/mm^{-1}	0.02	-4.25×10^{-3}
RMS spot size / μm	7.3 ± 0.7	2.7 ± 0.3

Optimising lenses with adaptive optics

Using aspheric surfaces, we slightly deformed the curved surface(s) of the plano-convex and bi-convex lens to reduce the RMS spot size further. Similar to before, objective functions were developed to feed into a minimisation routine that returns the optimal aspheric coefficients. This led to results in Table II, where the optimal aspheric coefficients are small as initially postulated. As seen in Fig 11, adaptive optics led to a significant spot size reduction for a biconvex lens (~ 10 times) but only a slight reduction for a plano-convex lens (15%).

TABLE II: Optimised adaptive optics parameters for lenses.

	Plano-convex lens	Biconvex lens
C_1/mm^{-1}	0.00	1.60×10^{-2}
C_2/mm^{-1}	0.02	-4.25×10^{-3}
$A_{4,1}$ / mm^{-3}	0.00	9.99×10^{-10}
$A_{6,1}$ / mm^{-5}	0.00	-4.86×10^{-7}
$A_{4,2}$ / mm^{-3}	9.53×10^{-7}	1.00×10^{-9}
$A_{6,2}$ / mm^{-5}	-4.72×10^{-8}	-5.41×10^{-7}
RMS spot size / μm	4.1 ± 0.4	0.20 ± 0.02

III. Conclusion & Further Work

The constructed optical ray tracer successfully modelled different optical systems using geometrical optics. A biconvex lens with optimal curvature parameters is the best for producing a sharp image. Adaptive optics further reduce the RMS spot size, especially for a biconvex lens. The diffraction effect becomes dominant at this smaller scale length, which should be modelled with Fourier optics. Other optical effects, such as reflection and dispersion, should also be incorporated into the existing model. Finally, it would be interesting to implement the adaptive optics code in a system where mirrors can be deformed in real time to reduce the RMS spot size. This an ongoing area of research in astronomy, where mirrors are deformed to remove aberrations due to atmospheric refraction.

References

[1] C. Pruss, E. Garbusi, and W. Osten, "Testing aspheres" *Optics and Photonics News*, vol. 19, no. 4, pp. 24–29, 2008.

[2] R. K. Tyson and B. W. Frazier, *Principles of adaptive optics*. CRC press, 2022.

[3] B. Brixner, "Lens design merit functions: rms image spot size and rms optical path difference," *Applied Optics*, vol. 17, no. 5, pp. 715–716, 1978

Appended Plots

Tracing ray trajectories through a convex surface

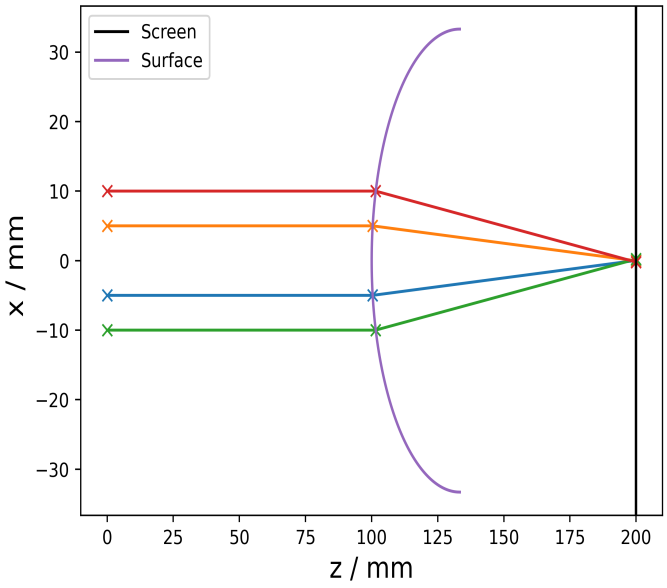

Fig. 1: Testing the model by tracing a few rays through a spherical surface placed at $z_0 = 100$ mm with $C = 0.03\ mm^{-1}$, $n_1 = 1$ and $n_2 = 1.5$. The rays converge at the expected focal point $f = z_0 + R\frac{n_2}{n_2 - n_1} = 200$ mm.

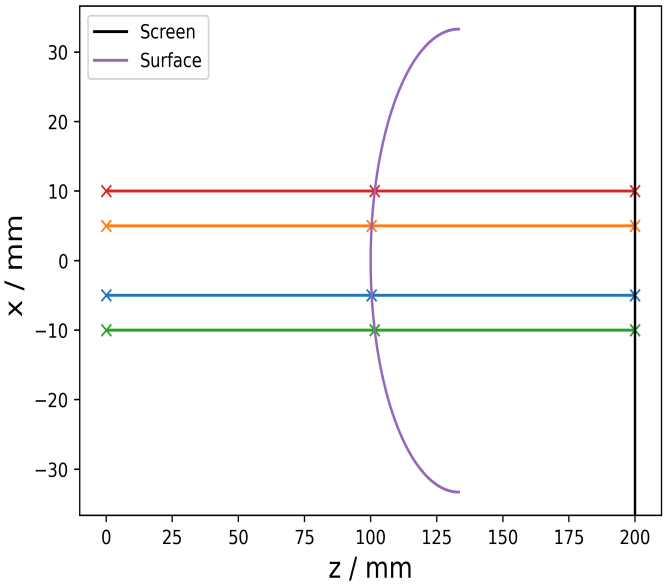

Fig. 3: Tracing rays through a surface with with $C = 0.03\ mm^{-1}$, $n_1 = n_2 = 1$, $z_0 = 100$, $r_{aperture} = 33.3$. No refraction occurs, as expected.

Simple test cases

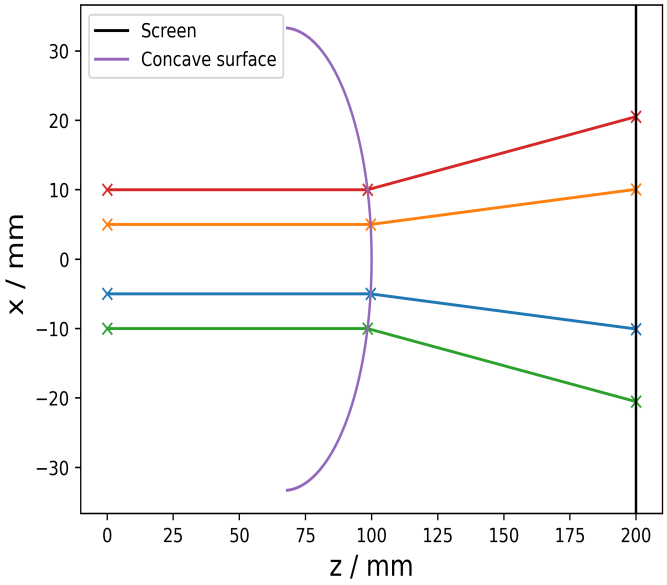

Fig. 2: Tracing paraxial rays through a concave surface with $C = -0.03\ mm^{-1}$, $n_1 = 1$ and $n_2 = 1.5$. Rays diverge, as expected.

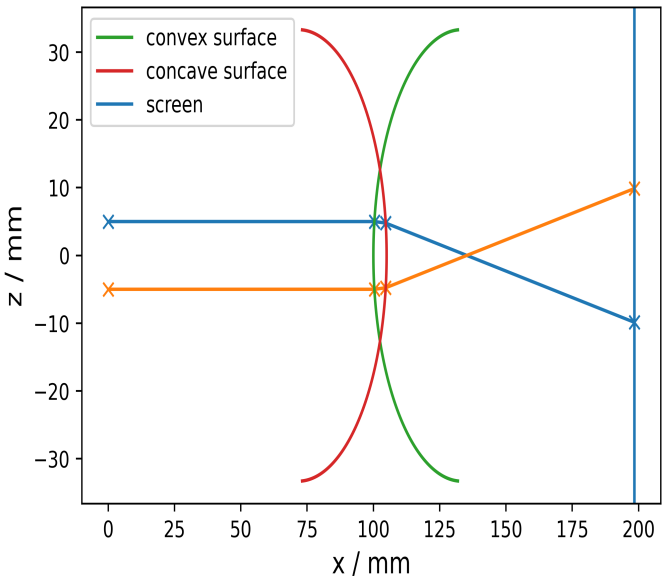

Fig. 4: Tracing rays through two surfaces separated by 5 mm with equal and opposite curvature of 0.03 mm^{-1}. The focal length is $\sim$ 32.7 mm, agreeing with the lens-maker equation $1/f = (n_{glass} - n_{air})(C_1 - C_2)$.

Tracing a collimated beam through a spherical surface

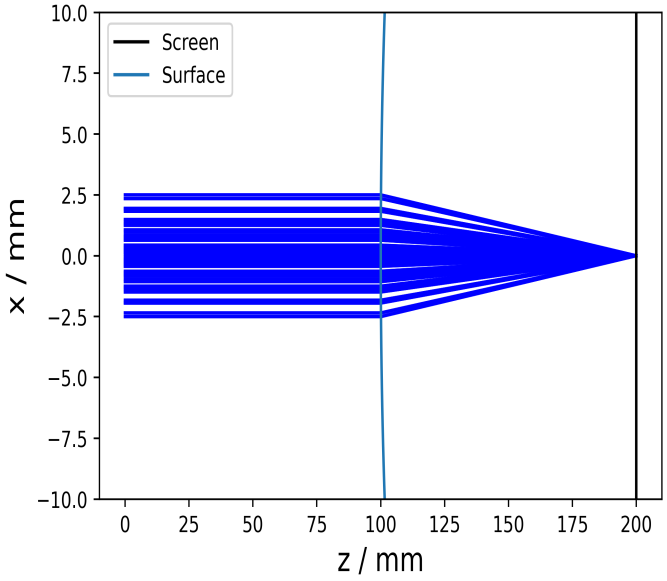

Fig. 5: Tracing a 5 mm collimated beam (100 rays) through a spherical surface with $C = 0.03\ mm^{-1}$, $n_1 = 1$, $n_2 = 1.5$, $z_0 = 100$, $r_{aperture} = 33.3$ mm. The beam converges at 200 mm, which is the expected focal point.

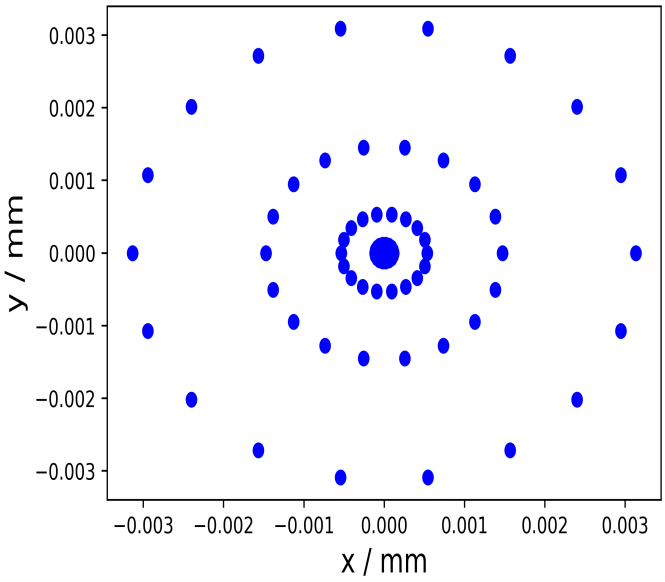

Fig. 7: Spot diagram at the focal plane $z = 200$ mm. For a sample ray number of 100, the RMS spot size is $\sim 1.6\ \mu m$.

Ray trajectories for the plano-convex lens in both orientations

Spot diagram for a 5 mm beam.

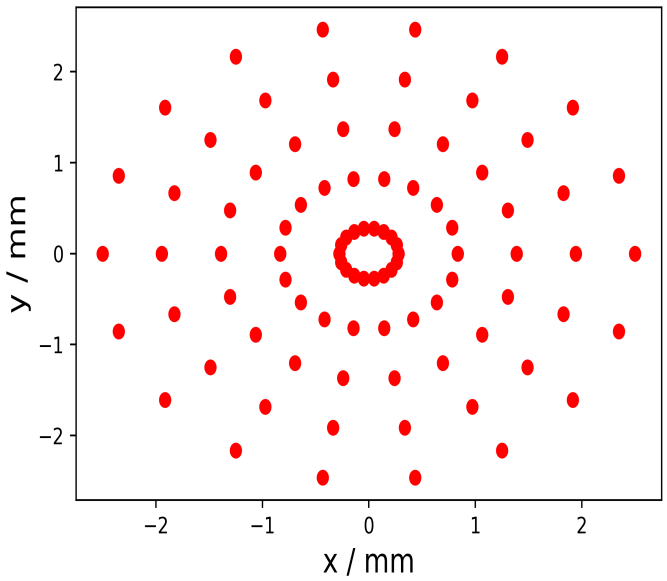

Fig. 6: Spot diagram at $z = 0$ mm. Notice the uniform distribution of the points to avoid biased RMS values.

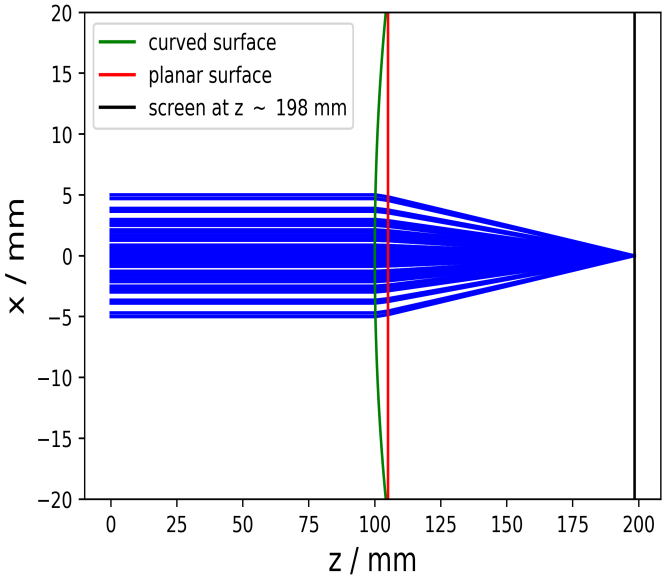

Fig. 8: Tracing 10 mm beam through a plano-convex lens (curved surface followed by planar surface orientation).

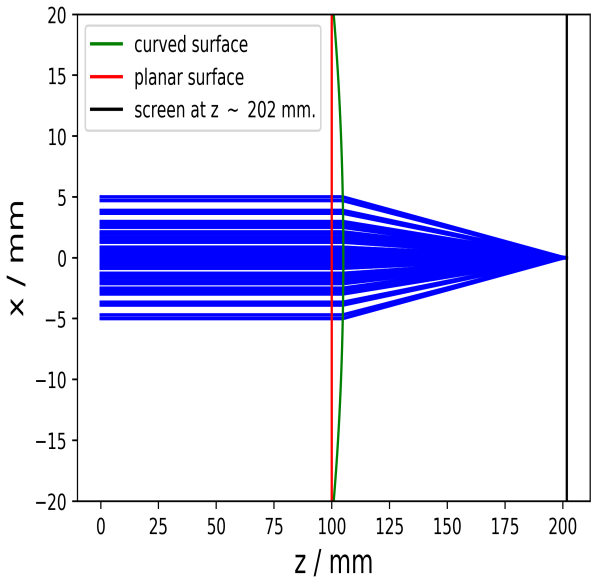

Fig. 9: Tracing 10 mm beam through a plano-convex lens (planar surface followed by curved surface orientation).

Comparing the performance of different lenses

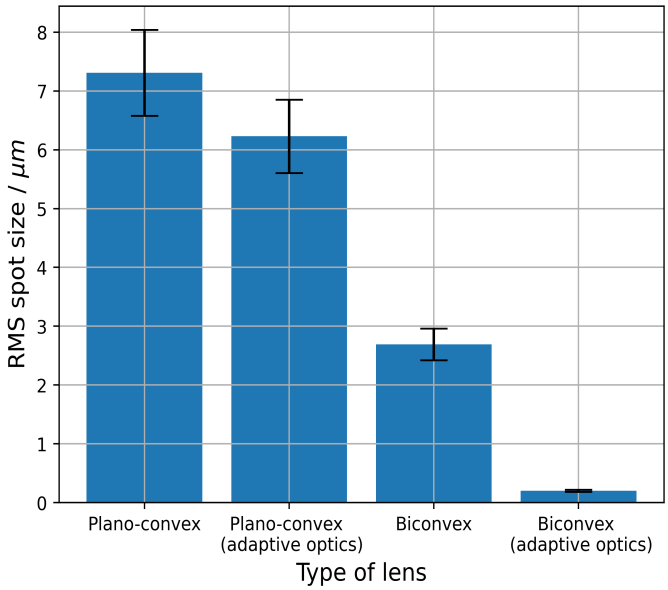

Fig. 11: Performance of different optical lenses for a 10 mm beam. The vertical error bars represent an uncertainty of 10% due to the small number of rays used (100).

Performance of the plano-convex lens

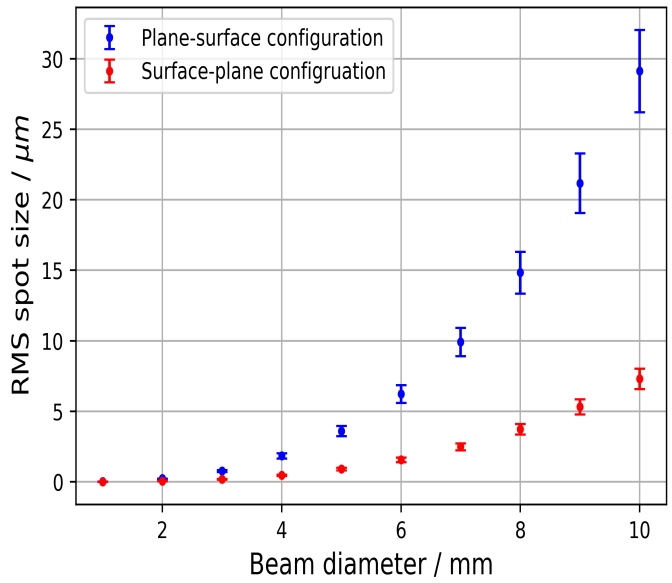

Fig. 10: Performance of plano-convex lens in both orientations for different beam diameters. The vertical error bars represent ±10% due to the small sample size (100 rays). Notice that the correct orientation is a convex surface followed by a planar surface (red).